Composites Science and Technology **44** (1992) 319–332

The influence of interphase regions on local thermal displacements in composites

N. R. Sottos*, R. L. McCullough

Department of Mechanical Engineering and Center for Composite Materials, University of Delaware, Newark, Delaware 19716, USA

&

W. R. Scott

Naval Air Development Center, Warminister, Pennsylvania 18974, USA

(Received 12 March 1991; revised version received 2 July 1991; accepted 1 August 1991)

Although the exact physical and chemical mechanisms are not clearly understood, it is widely believed that an interphase region with properties that differ from those of the plain matrix is developed near fiber surfaces in polymer matrix composites. The current study involves experimental investigation and theoretical modeling of the influence of the interphase on local thermal displacements. Experimental studies have centered on the development of a scanning microinterferometer for in-situ measurements of thermal displacements in the interphase. Thermal displacement measurements have been successfully made for specimens containing a single carbon fiber embedded in an epoxy matrix. A three-phase composite cylinder model is adopted to predict the thermal displacements of the single fiber specimen. Comparison of the theoretical displacement predictions with the experimental profiles measured by the interferometer indicate that the value of the matrix properties near the fiber surface differs from the value in the bulk resin. The data provide evidence of the existence of a lower glass transition temperature in the interphase.

Keywords: interphase, thermal, displacements, fiber/matrix interface, local properties

INTRODUCTION

A typical polymer composite consists of a reinforcement, either fibrous or particulate, embedded in a thermoplastic or thermoset matrix. It is widely believed that, when these constituents are combined into a composite, a third phase is formed. This phase has become known as the interphase. Hence, the interphase is defined as a region which develops between the constituents of a composite and possesses the properties neither of the reinforcement nor of the matrix. This region most probably has a gradient in material properties which approach those of the plain resin with radial distance. The size of the interphase has been estimated to be anywhere between a few nanometers and a few thousand.[1]

* To whom correspondence should be addressed: Present address: Department of Theoretical and Applied Mechanics, University of Illinois, Urbana, Illinois 61801, USA.

Composites Science and Technology 0266-3538/92/$05.00

In general, the interphase in polymer matrix composites can be formed by three basic mechanisms: chemical bonding, molecular segregation, and van der Waal bonding.[2] Through these mechanisms, structural gradients can be created in the matrix owing to the influence of the fiber surface on the long polymer chains.

In thermoplastic composites, an interphase can form as a result of segregation at the molecular level in the matrix. Schonhorn & Ryan[3] clearly demonstrated an enhancement of order development in polyethylene molecules in the vicinity of high-energy surfaces. Droste & DiBenedetto[4] observed a 9°C increase in the glass transition temperature of a thermoplastic polymer as the concentrations of particulate fillers were increased. This increase was interpreted as loss of long-range chain flexibility and mobility of the polymer molecules in the vicinity of the filler surface. Recently, Pangelinan[5] has shown that entropically driven molecular weight segregation occurs in a thermoplastic polymer owing to the presence of a surface. In addition, several researchers[6-9] have found that crystallization, nucleation, and transcrystallinity in thermoplastics are influenced by the fiber surface and are associated with the formation of an interphase.

In thermosetting systems, the interphase may result from changes in the cure chemistry of the resin near the fiber surface. Early on, Erickson *et al.*[10] proposed that the surface properties of glass fibers could cause some of the constituents in a thermosetting matrix to be adsorbed, deactivated or destroyed. An enrichment of the amine curing agent was shown to develop near the fiber surface. Lipatov *et al.*[11] demonstrated that fillers affect the relaxation time spectra of filled polymer systems. It was proposed that the presence of the filler restricted the molecular mobility of the epoxy matrix. Papanicolaou & Theocaris[12] used differential scanning calorimetry to measure changes in heat capacity with temperature for both a filled and an unfilled epoxy system. Estimates of an interphase volume fraction were based on differences in the jumps of the heat capacity of the two systems in the glass transition region. By means of infrared attenuated internal reflectance (IR) spectroscopy, Garton & Daly[13] showed that simulated reinforcement surfaces of both carbon and Aramid modify the cross-linking chemistry in the epoxy matrix adjacent to the surface.

More recently, Palmese[14] has shown that the presence of carbon fibers can alter the reaction behavior in thermosetting systems. Palmese performed extensive studies of the diffusion-related structural modifications of a Shell EPON 828/PACM 20 epoxy matrix. For this particular system, a stoichiometric imbalance of epoxy resin and amine curing agent developed near graphite fiber surfaces. The cross-link density, epoxy concentration and amine concentration were predicted as a function of radial distance from the fiber surface.

Although the interphase is of microscopic proportion, it actually constitutes a significant percentage of the matrix in a composite. The small-diameter fibers used in advanced composites have an extremely high surface area/volume ratio. For a high fiber volume fraction composite, this ratio is of the order of $10^4\,\text{in}^{-1}$.[2] Consequently, the fraction of the resin that is interphase can approach 50% in a typical 60% volume fiber composite. Thus, the structure and properties of the interphase have the potential to control many of the thermomechanical, chemical and electrical properties of the overall composite. In particular, the durability characteristics such as strength and fracture toughness are most likely to be affected.

Numerous papers have studied the influence of the interphase on mechanical performance of the composite. Review papers[1,15,16] discuss the importance of interphase constituents and chemistry, as well as the effects of interphase on overall composite strength, fracture, and environmental resistance. Parametric studies by Sottos *et al.*[17] have demonstrated that material property gradients in a thin interphase region around the fiber can have a significant effect on the development and distribution of local thermal stresses. Studies by Jayaraman & Reifsnider[18] have also found that gradients in the elastic modulus of the interphase alter the magnitude of the local stresses. Early studies by Arridge[19] demonstrated that an interphase can have a significant effect on the transverse stresses in fiber composites. More recently, Pagano & Tandon[20,21] and Tong & Jasiuk[22] have shown that the interphase strongly influences the transverse elastic stiffness of the composite.

It is believed that, by controlling the properties of the interphase, optimal composite properties and performance can be obtained. The ability to optimize the properties of the interphase effectively, however, relies on the ability to

predict or measure these property values. Determining the local structure and properties of the interphase is crucial to understanding how the interphase influences overall composite behavior. In order to develop and evaluate mechanics models or empirical relationships which correlate composite behavior with interphase behavior, the properties of the interphase must be accurately measured. Typical reinforcing fibers used in composite materials have diameters ranging from 5 μm to 150 μm, while the distance between fibers for a high volume fraction is of the order of 2 μm or less. Most of the traditional techniques for quantitatively determining material properties and behavior are inadequate for a region of this size. Consequently, the scale of micromechanical measurements must be refined to include the interphase region.

Recent investigations by Sottos *et al.*[23,24] and Ryan *et al.*[25] have demonstrated the utility of interferometric methods for non-destructively measuring thermal displacements in the interphase. Because an interferometer probe is a light beam, it has the capability to resolve small displacements in regions comparable to the wavelength of the light being used. The ability to make such displacement measurements provides a quantitative method for studying material properties and behavior on a microscale. It was proposed that, by measuring the displacements in a region local to the fiber and comparing them with theoretical predictions, trends in local material properties could be assessed. In this paper, an elasticity solution is derived for the prediction of the thermal displacements of a single fiber specimen. A three-phase composite cylinder model is adopted so that the influence of a uniform interphase region can be studied. The theoretical displacement profiles are compared with those measured by the interferometer, and several conclusions are made about the nature of the interphase in carbon/epoxy composites.

DISPLACEMENT MEASUREMENTS

Previous studies by Scott *et al.*[26,27] and Huber *et al.*[28] described a technique for measurement of sub-micron displacements caused by ultrasonic waves propagating at frequencies of 1 MHz and above. A distinguishing feature of these earlier methods was the formation of a magnified image on the face of a scanning detector, while the sample served as a stationary mirror in one arm of the interferometer. By using a scanning detector window with a diameter smaller than the obtainable resolution of the image, detailed displacement contour plots were made without the necessity for continuous realignment of the specimen. From these preliminary designs, a microinterferometric technique has evolved for measuring thermal displacements with an out-of-plane resolution of 5 nm and a possible in-plane resolution of 0·5 μm. A detailed description of the experimental technique is given by Sottos *et al.*[23,24] and Ryan *et al.*[25]

Table 1. Fiber and matrix material properties

Property	Carbon fiber	EPON 828/PACM 20
E (GPa)	41·0	2·5
α ($\times 10^{-6}$ °C^{-1})	−0·5	68·0
$K\left(\frac{W}{m°C}\right)$	8·3	0·18
ν	0·22	0·33

Thermal displacement measurements were obtained for specimens consisting of a single carbon fiber embedded in epoxy. The fibers used for this study were untreated 30-μm pitch-base carbon fibers supplied by Textron, the properties of which are listed in Table 1. The value for Young's modulus, E, was specified by the manufacturer, while the values for the longitudinal thermal expansion coefficient, α, thermal conductivity, K and Poisson's ratio, ν, were taken from the literature.[29] All of the fibers were washed in isopropyl alcohol to remove any surface residues before being used in a specimen. Shell EPON Resin 828 (diglycidyl ether of bisphenol A*) cured with a PACM 20 [bis(*p*-aminocyclohexyl)methane] amine was chosen as the matrix material. Properties of the plain resin are also given in Table 1. The modulus, Poisson's ratio and thermal conductivity were obtained from the manufacturer, while the coefficient of thermal expansion was determined from thermal mechanical analysis (TMA).[14]

Three samples, labeled A, B and C, were prepared for experimental analysis. Samples were made by placing a single fiber into the center of a mold which was then filled with a stoichiometric mix of resin (28 parts PACM 20:100 parts EPON 828). All samples were held for 1 h at 80°C to minimize the amount of bubbles in the resin phase, then cured for

30 min at 150°C, and allowed to cool slowly overnight to room temperature. Sample A was the first sample made and was cured separately several months prior to B and C. Specimens were cut to a length of approx. 2 cm and the front and back faces were polished metallographically. Polishing of the front face on which the measurements were made was critical to ensure a specularly reflective surface. The radius of the fiber was determined to be 17·2 μm from a photomicrograph of the sample surface. The outer radius of the samples measured 15·88 mm.

To heat the sample, a small current of 11·0 mA was passed through the fiber, as leads were attached to both the front and back polished faces of the specimen. A thin layer of gold was sputtered onto the surface to provide both a current conduction path and a highly reflective surface across the circular cross-section of the fiber/matrix interface. There were several advantages to heating the sample electrically in this manner. A repeatable, radial temperature field was generated in the sample which could be predicted analytically. The equilibrium time for heating and cooling the region of interest was small (typically less than 10 s). Finally, there was minimal convection of heat into the interferometer path, minimizing thermal effects on the apparatus.

Analytical prediction of the temperature distribution in the sample required the solution of the heat conduction equation for an electrically heated fiber embedded in an epoxy matrix. This problem has been solved previously[23] and the results are presented in the next section of this paper. By substituting the appropriate material properties into eqn (13), the analytical temperature distribution in the sample was calculated. A power input of 68 mW was used to heat the samples. As a result, the temperature in the fiber was nearly constant at 70°C, while the matrix temperature decreased rapidly away from the interface. The analytical prediction for fiber temperature was compared with experimental values and found to differ by less than 5%.[23]

To measure the thermal displacements at the interface, it was convenient to make measurements on single scan lines extending across the fiber center. The magnification of the interferometer was 25× for these measurements so that the far field matrix could be included in the scan. Heating the sample caused the matrix to expand upwardly and pull the fiber with it. Subtraction of an initial unheated scan line from the heated scan line yielded the net thermal displacement of the region. A series of displacement measurements was made on all three samples. Figure 1 is a plot of two consecutive displacement measurements on sample C. The displacements are plotted from the fiber center, $r = 0$, as a function of radial distance. The displacements have been normalized by subtracting from each point the value of the displacement of a reference point at 25 fiber radii out. The repeatability of the measurement on the same sample is excellent, as the largest difference between the two curves is approximately 15 nm. For both runs, the displacement of the fiber is nearly constant. However, there is a sharp rise in the displacement of the matrix near the interface, which peaks at about five fiber radii out. After this point, the matrix displacements decrease almost linearly with radial distance.

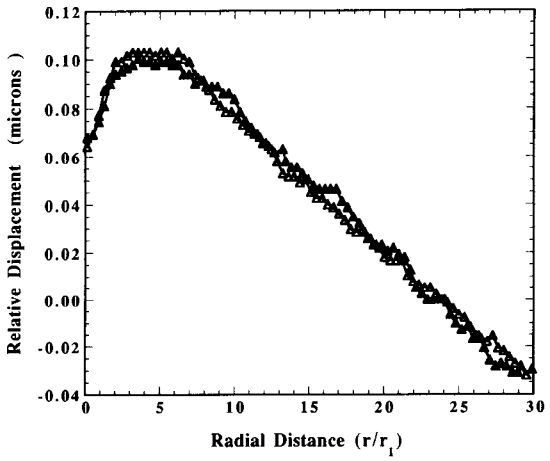

Fig. 1. Demonstration of repeatability of thermal displacement measurements for sample C.

The data for two consecutive runs on each sample were then averaged together and compared across samples. Figure 2 shows the average displacement profiles for samples A, B and C. Again, the displacements were normalized by a reference point 25 fiber radii out. The data from samples B and C show excellent repeatability. Although sample A exhibits the same trends as B and C, the difference in the profiles is much greater than the experimental accuracy. The anomalous results for sample A could be attributed to several factors. Sample A was cured separately from samples B and C. Moreover, sample A was mounted in the interferometer for approximately 6 months. During this time, it would have been able to

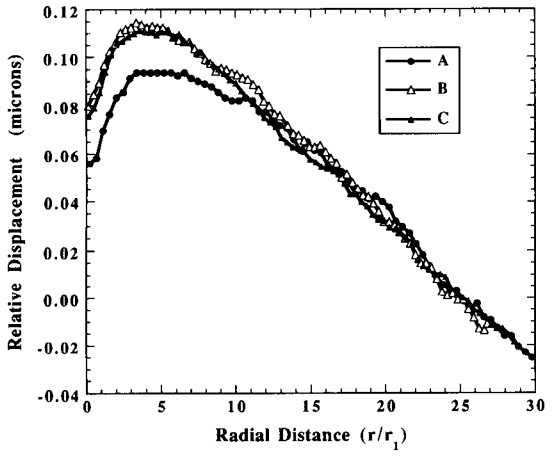

Fig. 2. Comparison of repeatability of thermal displacement measurements across samples A, B, C.

absorb appreciable moisture. Displacement measurements were recorded after several months of repeatedly scanning A to perfect the interferometer. The measurements on samples B and C were made within days of each other. Photomicrographs of the samples were taken after the experiments were completed. Sample A had a dark ring around the fiber which was not present in the other samples. In fact, the surfaces of samples B and C were so smooth that it was difficult to identify the fiber. It is not known whether the ring on sample A existed prior to making the displacement measurements. Since light is not reflected by such a ring, it would act to decrease the signal received by the photodetector and would significantly affect the measurement.

THEORETICAL PREDICTIONS

The literature contains a number of papers that derive a methodology for calculating the displacements and stresses in cylindrical domains. From linear thermoelasticity theory, Iesan[30] studied the static problem of thermal stresses and deformations in a composite cylinder made of two different homogeneous, isotropic materials. However, the analysis assumed that the out-of-plane (axial) displacements remained constant with radial distance. Although this assumption is acceptable when overall composite behavior is of concern, the variation can become significant when studying local material behavior. In fact, the radial variation of displacement is the precise quantity which was measured experimentally.

By using a two-phase, concentric cylinder model, Haener[31] predicted the stresses and displacements induced by both uniform resin shrinkage during processing and external loads in a unidirectional composite. The solution employed a potential approach, which did account for the radial dependence of axial displacement. By a similar method, Levy[32] developed a two-phase model to predict displacements resulting from an average applied load over the edge of the cylinder. The problem of thermal stresses in a hollow anisotropic cylinder due to axisymmetric temperature variations at the plane ends was solved by Misra & Achari[33] using potential functions of displacement. Additionally, Tanigawa & Kuriyama[34] have analyzed the transient thermal stresses and deformations in a semi-infinite solid cylinder with a moving boundary. The problem was treated as quasi-static state so that the temperature field and corresponding thermoelastic field could be analysed individually.

In the current study, a thermal displacement solution is derived for a three-phase, finite, composite cylinder model using a displacement potential approach. A schematic of the cylinder model is shown in Fig. 3. Throughout the analysis, the indices $i = 1, 2, 3$ will be used to denote the fiber, interphase and matrix domains, respectively. The interphase, $r_1 < r < r_2$, is treated as a region with uniform material properties, different from those of the matrix or the fiber. The matrix, fiber and interphase are assumed to be isotropic. This is a major assumption since the carbon fiber is actually

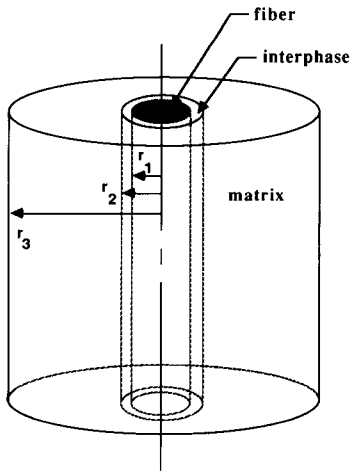

Fig. 3. Schematic of the three-phase finite cylinder model for the single fiber specimen.

transversely isotropic. Currently, no analytical tools exist for predicting the radial variation of axial displacement for a transversely isotropic fiber. Because the out-of-plane thermal displacements are dominated by the axial properties, the fiber properties chosen in Table 1 are the axial values.

The governing equation for the stationary thermoelastic problem in the ith domain is given by Nowacki[35] as

$$\hat{\mu}^{(i)}\nabla^2\mathbf{u}^{(i)} + (\hat{\lambda}+\hat{\mu})^{(i)}\,grad\,div\,\mathbf{u}^{(i)} + \mathbf{X}^{(i)} = \alpha^{(i)}\,grad\,T \quad (1)$$

where $\mathbf{u}$ is the displacement vector, T is the temperature distribution in the cylinder, α is the coefficient of thermal expansion, and $\hat{\lambda}$ and $\hat{\mu}$ are the Lamé constants. Because the cylinder is only subjected to a thermal load, the outer surfaces are traction free. This condition requires that at $z = l$

$$\sigma_z^{(i)} = 0, \qquad \sigma_{rz}^{(i)} = 0 \quad (2)$$

and at $r = r_3$

$$\sigma_r^{(3)} = 0, \qquad \sigma_{rz}^{(3)} = 0 \quad (3)$$

For both the fiber/interphase boundary, $r = r_1$, and the interphase/matrix boundary, $r = r_2$, continuity of displacements and tractions (perfect adhesion) is assumed. Thus the interface boundary conditions are expressed at $r = r_1$

$$u^{(1)} = u^{(2)}, \quad w^{(1)} = w^{(2)}, \quad \sigma_r^{(1)} = \sigma_r^{(2)}, \quad \sigma_{rz}^{(1)} = \sigma_{rz}^{(2)} \quad (4)$$

and at $r = r_2$

$$u^{(2)} = u^{(3)}, \quad w^{(2)} = w^{(3)}, \quad \sigma_r^{(2)} = \sigma_r^{(3)}, \quad \sigma_{rz}^{(2)} = \sigma_{rz}^{(3)} \quad (5)$$

The midplane of the cylinder is a plane of symmetry so that at $z = 0$

$$\sigma_{rz}^{(i)} = 0, \qquad w^{(i)} = 0 \quad (6)$$

A final boundary condition requires that the displacements are finite at the center of the fiber, $r = 0$.

Following the method of Nowacki,[35] the displacement solution is assumed to consist of two parts

$$\mathbf{u} = \mathbf{u}' + \mathbf{u}'' \quad (7)$$

where $\mathbf{u}'$ is the particular solution and $\mathbf{u}''$ is the complementary solution. (The superscripts (i) have been dropped temporarily for convenience.) The particular solution is given by

$$\mathbf{u}' = grad\,\Phi \quad (8)$$

where Φ is the displacement potential. Introducing eqns (7) and (8) into the governing eqn (1), the following relationship is obtained

$$grad[(\hat{\lambda}+2\hat{\mu})\nabla^2\Phi - \alpha T] + \hat{\mu}\nabla^2\mathbf{u}'' + (\hat{\lambda}+\hat{\mu})\,grad\,div\,\mathbf{u}'' = 0 \quad (9)$$

In order for eqn (9) to be valid, the following two characteristic equations must be satisfied:

$$\hat{\mu}\nabla^2\mathbf{u}'' + (\hat{\lambda}+\hat{\mu})\,grad\,div\,\mathbf{u}'' = 0 \quad (10)$$

$$\nabla^2\Phi = mT \quad (11)$$

where

$$m = \frac{\alpha}{\hat{\lambda}+2\hat{\mu}} \quad (12)$$

Thus the bounded problem can be solved in two steps. In the first step, a displacement potential, Φ, is determined from the solution of the Poisson eqn (11) by assuming a convenient boundary condition such as $\Phi = 0$. An expression for the temperature distribution in the cylinder, T, must be known. The heat conduction equation has been solved previously for the case of an electrically heated fiber embedded in an epoxy matrix. Neglecting heat losses from the outer surfaces of the sample at $r = r_2$ and $z = \pm l$, the steady-state temperature field in the sample is given as follows:[23]

$$T(r, z) = \sum_{n=1}^{\infty} [A_n I_0(\kappa_n r) + B_n K_0(\kappa_n r)]\cos(\kappa_n z) \quad (13)$$

where

$$A_n = Z_n K_0(\kappa_n r_2) \quad (14)$$

$$B_n = -Z_n I_0(\kappa_n r_2) \quad (15)$$

The constants Z_n are determined by the application of the boundary condition at $r = r_1$. This condition requires that there is no temperature discontinuity at the fiber/matrix interface. The constants are given by

$$Z_n = \frac{-4P}{n\pi\omega l}\left[\frac{\sin\left(\frac{n\pi}{2}\right)}{\left(\frac{2k_m\kappa_n F_1}{R_1}\right) - k_f\kappa_n^2 F_0}\right] \quad (16)$$

where

$$F_0 = K_0(\kappa_n r_1)I_0(\kappa_n r_2) - I_0(\kappa_n r_1)K_0(\kappa_n r_2) \quad (17)$$

$$F_1 = I_1(\kappa_n r_1)K_0(\kappa_n r_2) + K_1(\kappa_n r_1)I_0(\kappa_n r_2) \quad (18)$$

The functions, I_0, I_1 and K_0, K_1 are modified Bessel functions of the first and second kind, respectively. The κ_n are the eigenvalues and are expressed as

$$\kappa_n = \frac{n\pi}{2l} \quad (19)$$

Substitution of the temperature field given by eqn (13) into the right-hand side of eqn (11) yields the following displacement potential:[35]

$$\Phi = \frac{m}{2}\sum_{n=1}^{\infty}\frac{1}{\kappa_n^2}[A_n I_0(\kappa_n r) - B_n K_1(\kappa_n r)]\kappa_n r\cos(\kappa_n z) \quad (20)$$

The equations relating Φ to the particular components of the displacements are well known and are given in the appendix. Substitution of Φ into these relationships yields expressions for the particular displacements, $\mathbf{u}'$, and stresses, σ', which are also included in the appendix.

In the second step of the overall solution, the homogeneous eqn (10) is solved so that all the necessary boundary conditions are satisfied. The system of equations is solved conveniently in cylindrical coordinates using the Galerkin function, $\mathbf{F}$. Galerkin's representation has the form[35]

$$\mathbf{u}''^{(i)} = \frac{\hat{\lambda} + \hat{\mu}}{\hat{\lambda} + 2\hat{\mu}} grad\ div\ \mathbf{F} \quad (21)$$

where $\mathbf{F}$ is required to satisfy the biharmonic equation

$$\nabla^2\nabla^2\mathbf{F} = 0 \quad (22)$$

For the case when there is only a thermal load on the cylinder, the general solution to the biharmonic eqn (22) is given by[31]

$$\mathbf{F} = \sum_{n=1}^{\infty}[D_{1n}I_0(\kappa_n r) + D_{2n}K_0(\kappa_n r) + D_{3n}\kappa_n r I_1(\kappa_n r) + D_{4n}\kappa_n r K_1(\kappa_n r)]\sin(\kappa_n z) \quad (23)$$

where $D_{1n}^{(i)}$, $D_{2n}^{(i)}$, $D_{3n}^{(i)}$, and $D_{4n}^{(i)}$ are constants to be determined. The functions, I_0, I_1 and K_0, K_1 are modified Bessel functions of the first and second kind, respectively. The relationship of the complementary components of the displacements, $\mathbf{u}''$, and stresses, σ'', to the Galerkin vector, $\mathbf{F}$, are given in the appendix.

The superposition of the partial displacements, $\mathbf{u}'$ and $\mathbf{u}''$, and the partial stresses, σ' and σ'', yields the total displacements and stresses. In this manner, the final expression for axial displacement is as follows:

$$w^{(i)} = \sum_{n=1}^{\infty}[-\tfrac{1}{2}m^{(i)}rf_{1n} + D_{1n}^{(i)}h_{3n}^{(i)} + D_{2n}^{(i)}g_{3n}^{(i)} + D_{3n}^{(i)}h_{4n}^{(i)} + D_{4n}^{(i)}g_{4n}^{(i)}]\sin(\kappa_n z) \quad (24)$$

The functions, $h_{3n}^{(i)}$, $h_{4n}^{(i)}$, $g_{3n}^{(i)}$, $g_{4n}^{(i)}$ and f_{1n}, are given in the appendix. The twelve constants, $D_{1n}^{(i)}$, $D_{2n}^{(i)}$, $D_{3n}^{(i)}$, and $D_{4n}^{(i)}$, are determined by systematic application of the boundary conditions. It is important to note that the total stress, $\sigma = \sigma' + \sigma''$, and the total displacement, $\mathbf{u} = \mathbf{u}' + \mathbf{u}''$ must satisfy the boundary conditions.

The condition of finite displacements at $r = 0$ is applied first as it requires that $D_{2n}^{(1)} = 0$ and $D_{4n}^{(1)} = 0$. Next, the conditions at $z = l$ are imposed. Because the eigen-values, κ_n, are predetermined by the solution for the temperature field, the stresses $\sigma_z^{(i)}$ and $\sigma_{rz}^{(i)}$ do not vanish at the edge of the cylinder. According to Nowacki,[35] the stresses $\sigma_{rz}^{(i)}$ constitute a system in equilibrium, and the stresses $\sigma_z^{(i)}$ have the resultant

$$N = 2\pi\int\sigma_z^{(i)}r\,dr \quad (25)$$

Thus condition (2) can be satisfied by applying a uniform tension of magnitude $-N/A$ to the edge of the cylinder, where A is the cross-sectional area of the cylinder. Application of the remaining boundary conditions (3)–(6), creates a 10×10 system of linear algebraic equations. This set of equations can be written in matrix form and solved for the 10 remaining unknown constants by LU decomposition. Once the constants are determined, they are substituted in eqns (24) to calculate the theoretical value for axial displacement.

COMPARISON OF THEORY AND EXPERIMENT

By the use of eqn (24), the theoretical displacements could be calculated and compared with the experimental results. The necessary fiber and matrix properties are listed in Table 1. For a

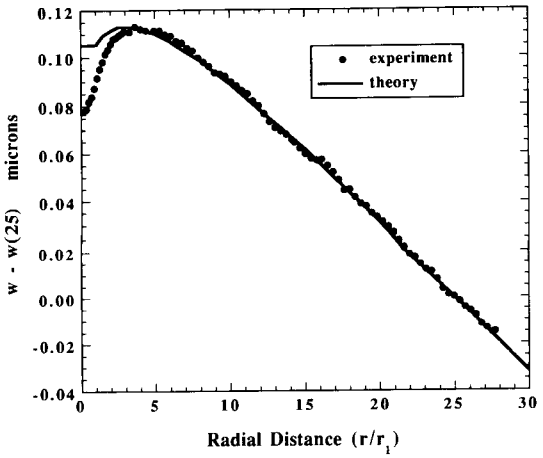

Fig. 4. Comparison of theoretical and experimental displacements for no interphase.

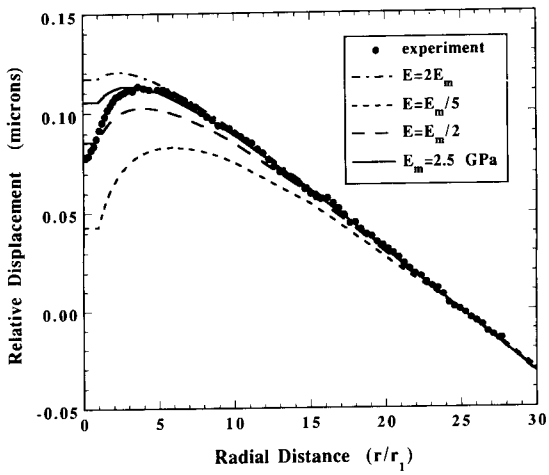

Fig. 5. Parametric studies of the effects of matrix modulus on the theoretical displacement profiles for no interphase.

first comparison, the influence of an interphase was not considered. The properties of the region, $r_1 < r < r_2$, were chosen to be identical to those of the surrounding matrix. In Fig. 4, the resulting theoretical displacement curve is plotted along with the experimental profile as a function of radial distance. The displacement values have again been normalized by subtracting the value of the displacement at twenty-five fiber radii out from the fiber. The experimental curve is the average of the data from two runs for samples B and C. From about three fiber radii out to the far field matrix, the theoretical and experimental predictions are in excellent agreement. At closer than three fiber radii to the fiber center, the two curves start to differ dramatically. The experimental value for the fiber displacement is much less than predicted by theory for a uniform matrix with no interphase. Consequently, there is a much sharper gradient in the experimental displacement curve at the fiber/matrix interface. When the sample is heated, the matrix material near the fiber surface does not behave as predicted for a uniform matrix with no interphase, while the matrix in the far field does behave as the bulk resin.

Before considering the influence of a distinct interphase, the effects of changing the material properties of the matrix were evaluated. Figure 5 demonstrates the effect of variations in the matrix modulus. As the modulus is changed from its measured value for the plain resin, the theoretical displacement profiles differ dramatically in the region from the fiber surface to about 15 fiber radii out into the matrix. As the modulus is made lower, the displacement profile near the fiber/matrix interface becomes steeper and approaches the gradient observed experimentally. This behavior is intuitive when the boundary conditions are considered. Continuity of displacements is required at the interface. Therefore, the lower the matrix modulus, the less the fiber is forced to extend with the matrix, and the steeper is the displacement gradient at the interface. Displacement profiles for different values of the matrix coefficient of thermal expansion are plotted in Fig. 6. Although different values of the expansion coefficient cause the slope of the far field displacement curve to change significantly, there is no pronounced influence on the displacement gradient at the interface. This preliminary parametric study

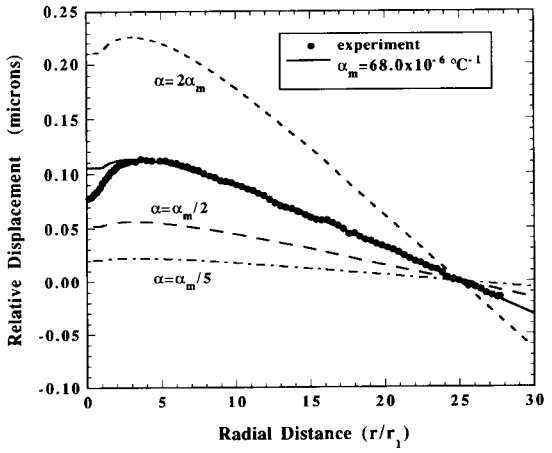

Fig. 6. Parametric studies of the effects of matrix coefficient of thermal expansion on the theoretical displacement profiles for no interphase.

suggests the existence of a low modulus region near the fiber surface.

Consequently, the next step in the analysis was to investigate the influence of a distinct interphase region with properties that varied significantly from the neat matrix. The thermal conductivity and Poisson's ratio of the interphase, however, were assumed to have the same values as the matrix. Three unknown variables, the interphase width, elastic modulus and coefficient of thermal expansion, were necessary to predict the thermal displacement field. Changes in the coefficient of thermal expansion of the interphase, had little influence on the displacement predictions unless unrealistically large interphase widths (over one fiber diameter) were considered. As expected from the above discussion on matrix modulus, decreasing the interphase modulus from the value for the plain resin caused the theoretical profiles to become much steeper at the fiber/matrix interface.

The value of the interphase modulus required to model the experimental profiles most closely was highly dependent on the chosen interphase width. As the width of the interphase region, $\lambda = r_2 - r_1$, was made smaller, a lower value of interphase modulus was needed to model the sharp displacement gradients observed experimentally. For larger interphase widths, the interphase modulus did not have to be quite as low to produce the necessary gradient. However, if too large an interphase width was chosen, the far field displacements would no longer correspond with the experimental profiles.

For thin interphase regions ($\lambda \leq 0{\cdot}5$ fiber radii), a modulus one order of magnitude lower than that of the plain resin most closely matched the experimental data. To obtain a modulus this low, the epoxy would have to be heated to a temperature above its glass transition, T_g. Polymers typically experience one order of magnitude drop in modulus accompanied by a two- or three-fold increase of the coefficient of thermal expansion at temperatures above their T_g. Palmese[14] has measured the value of the modulus and coefficient of thermal expansion above T_g for the EPON 828/PACM 20 system. These values are listed in Table 2. If the interphase parameters are assigned the values in Table 2, a value of $\lambda = 0{\cdot}058$ fiber radii as the interphase width most closely matches the experimental data.

Figure 7 compares the theoretical displacement

Table 2. EPON 828/PACM 20 material properties above T_g

E (GPa)	0·045
α ($\times 10^{-6}$ °C^{-1})	160·0

predictions with experimental observations for an interphase characterized by the properties in Table 2. The properties of the matrix were those of the plain resin given in Table 1. Although the experimental and theoretical values for fiber displacement are now comparable, the two curves do not match exactly. The theoretical curve is much steeper (almost vertical) at the fiber/matrix interface. If the physical gradients were as steep as predicted, there would be an averaging effect present in the experimental data owing to the size of the photodetector window. The window is 0·75 mm in diameter, which translates into 1·4 fiber radii on the magnified image plane. Thus any sharp change in profile will be averaged across the window. A schematic illustration of this 'windowing' effect on a vertical slope is shown in Fig. 8. Ideally, the experimental data should be deconvoluted to eliminate the effects of the circular detector window. It is much more convenient, however, to perform a running average of the theoretical displacement predictions. If the theoretical profile in Fig. 7 is averaged over the appropriate size window, the curve in Fig. 9 is obtained. The agreement between theory and experiment is improved even further. There is still a small discrepancy between

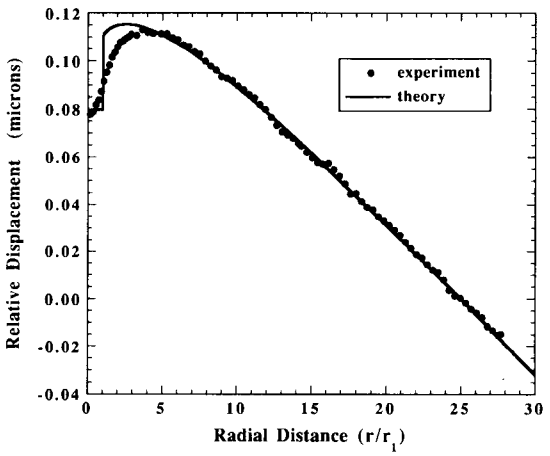

Fig. 7. Comparison of theoretical and observed displacement profiles for an interphase characterized by the parameters in Table 2.

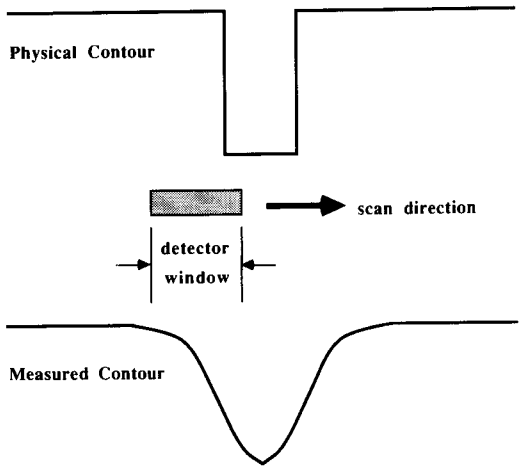

Fig. 8. Schematic illustration of 'windowing' effect on displacement profiles.

the two curves, but this may be attributed to the limitations of the theoretical displacement model. Only a uniform interphase region with no property gradients was considered. Ideally, a more sophisticated computational model of the thermal displacements could be developed to match more accurately the properties of the interphase. The current model, however, is sufficient to show the trends in the interphase properties needed to produce the measured displacement profiles.

DISCUSSION AND CONCLUSIONS

Comparison of the theoretical displacement predictions with the experimental profiles measured by the interferometer indicate that the value of the matrix properties near the fiber surface differed appreciably from the value in the plain resin. The difference between the experimental and theoretical curves when no interphase is considered is too large to be accounted for by experimental error or small variations in the properties of the matrix. A thin interphase region of approximately 0·06 fiber radii, with a modulus one order of magnitude lower than the plain resin, most closely matched the experimental profiles. In order for the modulus to be this low, the epoxy in the interphase would have to be heated to a temperature above its glass transition.

Recently, Palmese[14] has demonstrated that structural gradients occur near graphite fiber surfaces in the EPON 828/PACM 20 matrix which could potentially lower the glass transition temperature. Figure 10 is a plot of glass transition temperature as a function amine concentration for the EPON 828/PACM 20 system. At the stoichiometric point (28 parts PACM 20 : 100 parts EPON 828), the glass transition temperature is 160°C. For amine concentrations both above and below the stoichiometric point, the value of T_g is significantly reduced. If the fiber surface alters the cure chemistry such that a non-stoichiometric mixture of amine and epoxy occurs, the material in that region would have a much lower glass transition temperature than the plain resin. Hence it is possible that heating to 70°C during the experiment caused the material in a thin interphase to exceed its glass transition temperature. The surrounding matrix, sufficiently far from the fiber, would be

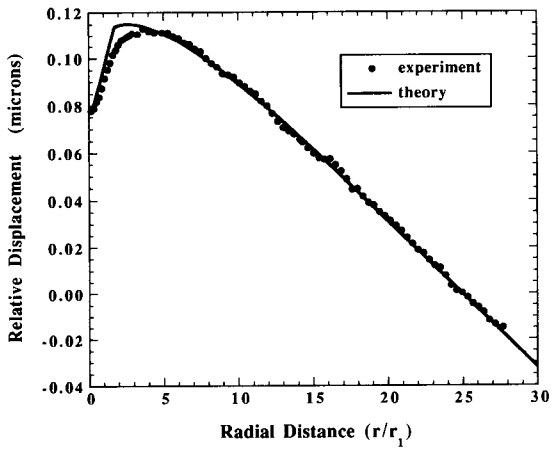

Fig. 9. Effect of 'windowing' theoretical thermal displacement predictions for interphase region characterized by the parameters in Table 2.

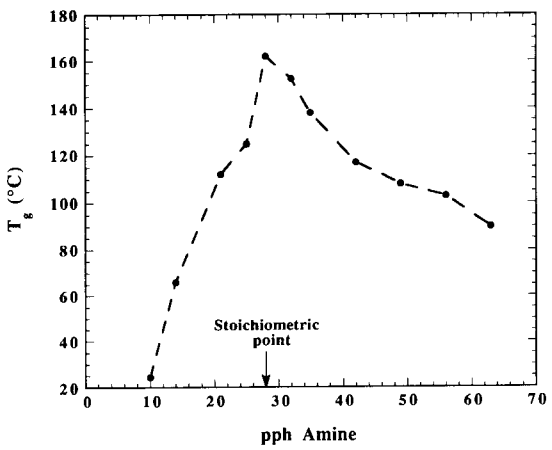

Fig. 10. Variation of glass transition temperature with amine concentration for a Shell EPON 828/PACM 20 epoxy matrix.

unaffected by this phenomenon. This result has significant implications for the thermal behavior and long-term performance of a composite.

The current study offers experimental evidence indicative of a depressed glass transition temperature in the interphase which is consistent with the findings of several other researchers. The concept of the existence of a viscoelastic interphase with a lower glass transition temperature has been discussed previously by Papanicolaou *et al.*[36] Pogany[37] first showed that non-stoichiometric concentrations of an aliphatic polyamine cross-linked with an epoxy resin can lead to reductions in the glass transition temperature. Lipatov *et al.*[11] concluded that a selective sorption of one of the components in a filled epoxy system may occur on the filler surface before hardening. A surplus of the other component may act as a plasticizer which causes a reduction of elastic moduli and a change in the relaxation behavior of the filled system. Crowson & Arridge[38] provided evidence for a difference in glass transition temperature between filled and unfilled epoxy systems.

Overall, an interferometric technique has been developed which is capable of making in-situ displacement measurements on a scale commensurate with the fiber/matrix unit cell. The ability to make such displacement measurements provides a quantitative method for studying material properties and behavior in the interphase. An elasticity solution was derived to predict the thermal displacements of a single fiber specimen. A three-phase model was adopted so that the influence of a uniform interphase region could be studied. Comparison of the theoretical displacement predictions with the experimental profiles measured by the interferometer verify that the value of the matrix properties do vary near the fiber surface. Furthermore, the experimental data imply that the interphase has a modulus significantly lower than that of the plain resin when heated, and consequently a lower glass transition temperature.

If the interphase has a lower glass transition temperature, the region would have a pronounced effect on the fracture toughness, durability and local stress state of the composite. Such a low modulus region would act to arrest crack growth in the matrix and significantly increase the fracture toughness. On the other hand, at high temperatures the performance of the composite would be significantly reduced. Work is in progress to control the interphase structures so that the interphase can be tailored to enhance or hinder these effects depending on the application.

ACKNOWLEDGEMENTS

This work was supported by an Office of Naval Research Fellowship and the Center for Composite Materials at the University of Delaware. The technical support and guidance of M. J. Ryan at APCOT Corp., Philadelphia, PA, and of Dr S. Güçeri at the Department of Mechanical Engineering, University of Delaware, as well as the use of the facilities at the Naval Air Development Center, Warminster, PA, are greatly appreciated.

REFERENCES

1. Drzal, L. T., The interphase in epoxy composites. *Advances in Polymer Science,* **75** (1986) 1–32.
2. McCullough, R. L., *Concepts of Fiber-Resin Composites.* Marcel Dekker, Inc., New York, 1971.
3. Schonhorn, H. & Ryan, F. W., Surface structure of polymers: Glancing angle electron diffraction study of polyethylene. *Journal of Applied Polymer Science,* **6** (1968) 231.
4. Droste, D. H. & DiBenedetto, A. T., The glass transition temperature of filled polymers and its effect on their physical properties. *Journal of Polymer Science,* **13** (1969) 2149–59.
5. Pangelinan, A. P., Surface induced molecular weight segregation in thermoplastic composites. PhD thesis, Department of Chemical Engineering, University of Delaware, Newark, Delaware, 1991.
6. Bessel, T. & Shortall, J. B., The crystallization and interfacial bond strength of nylon 6 at carbon and glass fibre surfaces. *Journal of Material Science,* **10** (1975) 2035–49.
7. Burton, R. H. & Folkes, M. J., Interfacial morphology in short fibre reinforced thermoplastics. *Plastic Rubber Processing Applications,* **3** (1983) 129.
8. Burton, R. H., Day, T. M. & Folkes, M. J., Localized flow induced morphological features in fibre reinforced thermoplastics. *Polymer Communications,* **25** (1984) 361.
9. Hobbs, S. Y., Row nucleation of isotatic polypropylene. *Nature, Physical Sciences,* **234** (1971) 12.
10. Erickson, P. W., Volpe, A. & Cooper, E. R., Chemical and physical effects of glass surfaces upon laminating resins. In *Proceedings of the 19th Conference SPI,* Section 21-A, 1966.
11. Lipatov, Y. S., Babich, V. F. & Rosovizky, V. F., Effect of filler on the relaxation time spectra of filled polymers. *Journal of Applied Polymer Science,* **20** (1976) 1787–94.
12. Papanicolaou, G. C. & Theocaris, P. S., Thermal properties and volume fraction of the boundary

interphase in metal-filled epoxies. *Colloid and Polymer Science,* **257** (1979) 239–46.
13. Garton, A. & Daly, J. H., Characterization of the aramid: Epoxy and interphases. *Polymer Composites,* **6**(4) (1985) 195–9.
14. Palmese, G. R., The interphase in thermosetting composites. PhD thesis, Department of Chemical Engineering, University of Delaware, Newark, Delaware, 1991.
15. Hughes, J. D. H., The carbon fibre/epoxy interface: a review. *Composites Science and Technology,* **41** (1991) 13–45.
16. Swain, R. E., Reifsnider, K. L., Jayaraman, K. & El-Zein, M., Interface/interphase concepts in composite material systems. *Journal of Thermoplastic Composite Materials,* **3** (1990) 13–23.
17. Sottos, N. R., McCullough, R. L. & Güçeri, S. I., Thermal stresses due to property gradients at the fiber/matrix interface. In *Mechanics of Composite Materials and Structures,* vol. AMD-100, ed. J. N. Reddy & J. L. Teply. ASME, New York, Special Volume, 1989.
18. Jayaraman, K. & Reifsnider, K. L., Micromechanical stress analysis of continuous-fiber composites with local material property gradients. In *Proceedings of the Fifth Japan–U.S. Conference on Composite Materials,* Technomic, Lancaster, PA, 1990.
19. Arridge, R. G. C., The effect of interlayers on the transverse stresses in fiber composites. *Polymer Engineering Science,* **15**(10) (1975) 757–60.
20. Pagano, N. J. & Tandon, G. P., Thermo-elastic model of multi-directional coated-fiber composites: Traction formulation. *Composites Science and Technology,* **38** (1990) 247–69.
21. Pagano, N. J. & Tandon, G. P., Elastic response of multi-directional coated-fiber composites. *Composites Science and Technology,* **31** (1988) 273–93.
22. Tong, Y. & Jasiuk, I., The effect of interface on the mechanical properties of composites. In *Interfaces in Polymer, Ceramic, and Metal Matrix Composites,* ed. H. Ishida. Elsevier Science Publishers, New York, 1988, pp. 757–64.
23. Sottos, N. R., Scott, W. R. & McCullough, R. L., Micro-interferometry for measurement of thermal displacements at fiber/matrix interfaces. *Experimental Mechanics,* **31**(2) (1991) 98–103.
24. Sottos, N. R., Scott, W. R. & Ryan, M. J., Repeatability of local thermal displacement measurements near the fiber/matrix interface using micro-interferometry. In *Review of Progress in Quantitative Nondestructive Evaluation,* vol. 10A, ed. D. O. Thompson & D. E. Chimenti, Plenum Press, New York, 1990, pp. 1057–63.
25. Ryan, M. J., Scott, W. R. & Sottos, N. R., Scanning heterodyne microinterferometry for high resolution contour mapping. In *Review of Progress in Quantitative Nondestructive Evaluation,* vol. 10B, ed. D. O. Thompson & D. E. Chimenti, Plenum Press, New York, 1990, pp. 2069–75.
26. Scott, W. R., Huber, S. & Ryan, M., An image scanning heterodyne microinterferometer. In *Review of Progress in Quantitative Nondestructive Evaluation,* vol. 7B, ed. D. O. Thompson & D. E. Chimenti, Plenum Press, New York, 1988, pp. 1065–73.
27. Scott, W. R., Ryan, M. J., Granata, D. M. & Sottos, N. R., Nondestructive evaluation and characterization of composite materials microinterferometry. In *1st Navy Independent Research/Independent Exploratory Development Symposium,* vol. 1, ed. D. S. Eggleston, Chemical Propulsion Information Agency, Laurel, 1988, pp. 481–91.
28. Huber, S., Scott, W. R. & Sands, R., Detection and analysis of waves propagating in boron/aluminum composite materials. In *Review of Progress in Quantitative Nondestructive Evaluation,* vol. 6B, ed. D. O. Thompson & D. E. Chimenti, Plenum Press, New York, 1987, pp. 1065–73.
29. Chamis, C. C., Mechanics of load transfer at the interface. In *Composite Materials,* vol. 6, ed. E. P. Pluddemann, Academic Press, New York, 1974, pp. 32–77.
30. Iesan, D., Thermal stresses in composite cylinders. *Journal of Thermal Stresses,* **3** (1980) 495–508.
31. Haener, J., Micromechanical behavior of fiber reinforced plastics. Technical Report 66-62, USAAVLABS, 1966. AD-643813.
32. Levy, A., Fiber–matrix interaction in a composite material. Technical Report N70-24467, Grumman Research Department, 1970.
33. Misra, J. C. & Achari, R. M., On axisymmetric thermal stresses in an anisotropic hollow cylinder. *Journal of Thermal Stresses,* **3** (1980) 509–20.
34. Tanigawa, Y. & Kuriyama, S., Transient thermal stresses and thermal deformations in a solid cylinder with a moving boundary. *Ingenieur-Archiv,* **55** (1985) 221–35.
35. Nowacki, W., *Thermoelasticity.* Addison-Wesley Publishing Co., Reading, Massachusetts, 1986.
36. Papanicolaou, G. C., Paipetis, S. A. & Theocaris, P. S., The concept of boundary interphase in composite mechanics. *Colloid and Polymer Science,* **256** (1978) 625–30.
37. Pogany, G. A., The β-relaxation in epoxy resins, the temperature and time-dependence of cure. *Journal of Materials Science,* **4** (1969) 405–9.
38. Crowson, R. J. & Arridge, R. G. C., The elastic properties in bulk and shear of a glass bead-reinforced epoxy resin composite. *Journal of Materials Science,* **12** (1977) 2154–64.
39. Boresi, A. P. & Chong, K. P., *Elasticity in Engineering Mechanics.* Elsevier Science Publishing Co., Inc., New York, 1987.

APPENDIX

In general, the displacements and stress components associated with the particular solution are related to Φ in cylindrical coordinates by[39]

$$u' = \frac{\partial \Phi}{\partial r} \tag{A1}$$

$$w' = \frac{\partial \Phi}{\partial z} \tag{A2}$$

$$\sigma_r' = 2\hat{\mu}\left(\frac{\partial^2 \Phi}{\partial^2 r} - \nabla^2 \Phi\right) \tag{A3}$$

$$\sigma_z' = 2\hat{\mu}\left(\frac{\partial^2 \Phi}{\partial^2 z} - \nabla^2 \Phi\right) \tag{A4}$$

$$\sigma_\theta' = 2\hat{\mu}\left(\frac{1}{r}\frac{\partial \Phi}{\partial r} - \nabla^2 \Phi\right) \tag{A5}$$

$$\sigma'_{rz} = 2\hat{\mu}\left(\frac{\partial^2 \Phi}{\partial r\, \partial z}\right) \tag{A6}$$

Substitution of Φ, given by eqn (20), into the relationships (A1)–(A6) yields the following expressions for the corresponding components of the stresses and displacements:

$$u'^{(i)} = \frac{m^{(i)}}{2} \sum_{n=1}^{\infty} r f_{0n}(r) \cos(\kappa_n z) \tag{A7}$$

$$w'^{(i)} = -\frac{m^{(i)}}{2} \sum_{n=1}^{\infty} r f_{1n}(r) \sin(\kappa_n z) \tag{A8}$$

$$\sigma_r'^{(i)} = \hat{\mu}^{(i)} m^{(i)} \sum_{n=1}^{\infty} \times [\kappa_n r f_{1n}(r) - f_{0n}(r)] \cos(\kappa_n z) \tag{A9}$$

$$\sigma_{rz}'^{(i)} = -\hat{\mu}^{(i)} m^{(i)} \sum_{n=1}^{\infty} \kappa_n r f_{0n}(r) \sin(\kappa_n z) \tag{A10}$$

$$\sigma_\theta'^{(i)} = -\hat{\mu}^{(i)} m^{(i)} \sum_{n=1}^{\infty} f_{0n} \cos(\kappa_n z) \tag{A11}$$

$$\sigma_z'^{(i)} = -\hat{\mu}^{(i)} m^{(i)} \sum_{n=1}^{\infty} \times [\kappa_n r f_{1n}(r) + f_{0n}(r)] \cos(\kappa_n z) \tag{A12}$$

where

$$f_{0n}(r) = [A_n I_0(\kappa_n r) + B_n K_0(\kappa_n r)] \tag{A13}$$

$$f_{1n}(r) = [A_n I_1(\kappa_n r) - B_n K_1(\kappa_n r)] \tag{A14}$$

The constants A_n and B_n are the same as given in eqns (14) and (15).

For a cylindrically symmetric coordinate system, the components of the displacements and stresses associated with the complementary solution are related to the Galerkin vector, $\mathbf{F}$, by[35]

$$u'' = -\frac{1}{1-2\nu}\left[\frac{\partial^2 \mathbf{F}}{\partial r\, \partial z}\right] \tag{A15}$$

$$w'' = \frac{1}{1-2\nu}\left[2(1-\nu)\nabla^2 \mathbf{F} - \frac{\partial^2 \mathbf{F}}{\partial z^2}\right] \tag{A16}$$

$$\sigma_r'' = \frac{2\hat{\mu}}{1-2\nu}\frac{\partial}{\partial z}\left[\nu \nabla^2 \mathbf{F} - \frac{\partial^2 \mathbf{F}}{\partial r^2}\right] \tag{A17}$$

$$\sigma_\theta'' = \frac{2\hat{\mu}}{1-2\nu}\frac{\partial}{\partial z}\left[\nu \nabla^2 \mathbf{F} - \frac{1}{r}\frac{\partial \mathbf{F}}{\partial r}\right] \tag{A18}$$

$$\sigma_{rz}'' = \frac{2\hat{\mu}}{1-2\nu}\frac{\partial}{\partial r}\left[(1-\nu)\nabla^2 \mathbf{F} - \frac{\partial^2 \mathbf{F}}{\partial z^2}\right] \tag{A19}$$

$$\sigma_z'' = \frac{2\hat{\mu}}{1-2\nu}\frac{\partial}{\partial z}\left[(2-\nu)\nabla^2 \mathbf{F} - \frac{\partial^2 \mathbf{F}}{\partial z^2}\right] \tag{A20}$$

Substitution of $\mathbf{F}$, given by eqn (23), into the relationships (A15)–(A20), yields the following expressions for the corresponding components of the stresses and displacements:

$$u''^{(i)} = \sum_{n=1}^{\infty} [D_{1n}^{(i)} h_{1n}^{(i)}(r) + D_{2n}^{(i)} g_{1n}^{(i)}(r) + D_{3n}^{(i)} h_{2n}^{(i)}(r) + D_{4n}^{(i)} g_{2n}^{(i)}(r)] \cos(\kappa_n z) \tag{A21}$$

$$w''^{(i)} = \sum_{n=1}^{\infty} [D_{1n}^{(i)} h_{3n}^{(i)}(r) + D_{2n}^{(i)} g_{3n}^{(i)}(r) + D_{3n}^{(i)} h_{4n}^{(i)}(r) + D_{4n}^{(i)} g_{4n}^{(i)}(r)] \sin(\kappa_n z) \tag{A22}$$

$$\sigma_r''^{(i)} = \sum_{n=1}^{\infty} [D_{1n}^{(i)} h_{5n}^{(i)}(r) + D_{2n}^{(i)} g_{5n}^{(i)}(r) + D_{3n}^{(i)} h_{6n}^{(i)}(r) + D_{4n}^{(i)} g_{6n}^{(i)}(r)] \cos(\kappa_n z) \tag{A23}$$

$$\sigma_\theta''^{(i)} = \sum_{n=1}^{\infty} [D_{1n}^{(i)} h_{7n}^{(i)}(r) + D_{2n}^{(i)} g_{7n}^{(i)}(r) + D_{3n}^{(i)} h_{8n}^{(i)}(r) + D_{4n}^{(i)} g_{8n}^{(i)}(r)] \cos(\kappa_n z) \tag{A24}$$

$$\sigma_z''^{(i)} = \sum_{n=1}^{\infty} [D_{1n}^{(i)} h_{9n}^{(i)}(r) + D_{2n}^{(i)} g_{9n}^{(i)}(r) + D_{3n}^{(i)} h_{10n}^{(i)}(r) + D_{4n}^{(i)} g_{10n}^{(i)}(r)] \cos(\kappa_n z) \tag{A25}$$

$$\sigma_{rz}''^{(i)} = \sum_{n=1}^{\infty} [D_{1n}^{(i)} h_{11n}^{(i)}(r) + D_{2n}^{(i)} g_{11}^{(i)}(r) + D_{3n}^{(i)} h_{12n}^{(i)}(r) + D_{4n}^{(i)} g_{12}^{(i)}(r)] \cos(\kappa_n z) \tag{A26}$$

where $D_{1n}^{(i)}$, $D_{2n}^{(i)}$, $D_{3n}^{(i)}$, and $D_{4n}^{(i)}$ are constants to be determined. The functions $h_{jn}^{(i)}$ and $g_{jn}^{(i)}$, where $j = 1, 2, \ldots, 12$, are combinations of modified Bessel functions and can be expressed in terms of the engineering constants, E and ν, as follows:

$$h_{1n}^{(i)} = -\left(\frac{1+\nu^{(i)}}{E^{(i)}}\right)\kappa_n^2 I_1(\kappa_n r) \tag{A27}$$

$$h_{2n}^{(i)} = \left(-\frac{1+\nu^{(i)}}{E^{(i)}}\right)\kappa_n^3 r I_0(\kappa_n r) \tag{A28}$$

$$h_{3n}^{(i)} = \left(\frac{1+\nu^{(i)}}{E^{(i)}}\right)\kappa_n^2 I_0(\kappa_n r) \tag{A29}$$

$$h_{4n}^{(i)} = \left(\frac{1+\nu^{(i)}}{E^{(i)}}\right)\kappa_n^2 \times [4(1-\nu) I_0(\kappa_n r) + \kappa_n r I_1(\kappa_n r)] \tag{A30}$$

$$h_{5n}^{(i)} = \kappa_n^2\left[-\kappa_n I_0(\kappa_n r) + \frac{1}{r} I_1(\kappa_n r)\right] \tag{A31}$$

$$h_{6n}^{(i)} = \kappa_n^3[(2\nu - 1) I_0(\kappa_n r) - \kappa_n r I_1(\kappa_n r)] \tag{A32}$$

$$h_{7n}^{(i)} = -\kappa_n^2 \frac{1}{r} I_1(\kappa_n r) \tag{A33}$$

$$h_{8n}^{(i)} = \kappa_n^3 (2\nu - 1) I_0(\kappa_n r) \tag{A34}$$

$$h_{9n}^{(i)} = \kappa_n^3 I_0(\kappa_n r) \tag{A35}$$

$$h_{10n}^{(i)} = \kappa_n^3 [2(2 - \nu) I_0(\kappa_n r) + \kappa_n r I_1(\kappa_n r)] \tag{A36}$$

$$h_{11n}^{(i)} = \kappa_n^3 I_1(\kappa_n r) \tag{A37}$$

$$h_{12n}^{(i)} = \kappa_n^3 [\kappa_n r I_0(\kappa_n r) + 2(1 - \nu) I_1(\kappa_n r)] \tag{A38}$$

$$g_{1n}^{(i)} = \left(\frac{1 + \nu^{(i)}}{E^{(i)}}\right) \kappa_n^2 K_1(\kappa_n r) \tag{A39}$$

$$g_{2n}^{(i)} = \left(\frac{1 + \nu^{(i)}}{E^{(i)}}\right) \kappa_n^3 r K_0(\kappa_n r) \tag{A40}$$

$$g_{3n}^{(i)} = \left(\frac{1 + \nu^{(i)}}{E^{(i)}}\right) \kappa_n^2 K_0(\kappa_n r) \tag{A41}$$

$$g_{4n}^{(i)} = \left(\frac{1 + \nu^{(i)}}{E^{(i)}}\right) \times \kappa_n^2 [-4(1 - \nu) K_0(\kappa_n r) + \kappa_n r K_1(\kappa_n r)] \tag{A42}$$

$$g_{5n}^{(i)} = \kappa_n^2 \left[-\kappa_n K_0(\kappa_n r) - \frac{1}{r} K_1(\kappa_n r) \right] \tag{A43}$$

$$g_{6n}^{(i)} = \kappa_n^3 [(1 - 2\nu) K_0(\kappa_n r) - \kappa_n r K_1(\kappa_n r)] \tag{A44}$$

$$g_{7n}^{(i)} = \kappa_n^2 \frac{1}{r} K_1(\kappa_n r) \tag{A45}$$

$$g_{8n}^{(i)} = \kappa_n^3 (1 - 2\nu) K_0(\kappa_n r) \tag{A46}$$

$$g_{9n}^{(i)} = \kappa_n^3 K_0(\kappa_n r) \tag{A47}$$

$$g_{10n}^{(i)} = \kappa_n^3 [-2(2 - \nu) K_0(\kappa_n r) + \kappa_n r K_1(\kappa_n r)] \tag{A48}$$

$$g_{11n}^{(i)} = -\kappa_n^3 K_1(\kappa_n r) \tag{A49}$$

$$g_{12n}^{(i)} = \kappa_n^3 [-\kappa_n r K_0(\kappa_n r) + 2(1 - \nu) K_1(\kappa_n r)] \tag{A50}$$